Energy 301 (2024) 131756

Contents lists available at ScienceDirect

Energy

journal homepage: www.elsevier.com/locate/energy

Numerical investigation and optimization of a hexagonal thermoelectric generator with diverging fins for exhaust waste heat recovery

Ding Luo [a,b,**], Haokang Zhang [a], Jin Cao [a], Yuyin Yan [c], Bingyang Cao [b,*]

[a] Collaborative Innovation Center for Microgrid of New Energy, College of Electrical Engineering & New Energy, China Three Gorges University, Yichang, China
[b] Key Laboratory for Thermal Science and Power Engineering of Ministry of Education, Department of Engineering Mechanics, Tsinghua University, Beijing, 100084, China
[c] Faculty of Engineering, University of Nottingham, University Park, Nottingham, UK

ARTICLE INFO

Keywords:
Thermoelectric generator
Waste heat recovery
Temperature uniformity
Pressure drop
Numerical simulation

ABSTRACT

Conventional thermoelectric generator (TEG) configurations suffer from the temperature drop of exhaust gas, resulting in a decrease in output power. To address this issue, diverging fins are introduced into a hexagonal TEG to enhance the heat transfer between exhaust gas and heat exchanger. Additionally, a corresponding numerical model is established to predict and optimize the output performance of the hexagonal TEG. The study indicates that, as the diverging angle, number, and height of diverging fins increase, both output power and pressure drop of the hexagonal TEG continuously increase, except for the pressure drop which decreases with the increase of fin height. To achieve maximum output power, the optimal values for fin height (h) and number (n) are determined to be 15 mm and 30, respectively. Moreover, regarding the diverging angle, the optimal value is related to the exhaust mass flow rate, and the optimal diverging angle is 0.2° when the flow rate is lower than 35 g/s. At an exhaust mass flow rate of 35 g/s and a temperature of 550 K, the optimal hexagonal TEG achieves an output power of 143.94 W, experiencing a 5.83 % improvement compared to the traditional structure. Meanwhile, the pressure drop is only 1.92 kPa, within the allowable range of the hexagonal TEG. This research provides new perspectives for enhancing the performance of TEGs by introducing diverging fins in heat exchangers.

Nomenclature

Abbreviations

CFD	computational fluid dynamics
TEG	thermoelectric generator
TEM	thermoelectric module

Symbols

A	area, m^2
D	diameter, mm
$\vec{E}$	electric field density vector, $V{\cdot}m^{-2}$
h	height, mm
$\vec{J}$	current density vector, $A{\cdot}m^{-2}$
k	turbulent kinetic energy, $m^2{\cdot}s^{-2}$
U	voltage, V
$\vec{v}$	velocity, $m{\cdot}s^{-1}$

Greek symbols

α	diverging angle, °
σ^{-1}	electrical resistivity, Ω·m
φ	electrical potential, V
ε	turbulent dissipation rate, $m^2{\cdot}s^{-3}$
ρ	density, $kg{\cdot}m^{-3}$
μ	dynamic viscosity, Pa·s
λ	thermal conductivity, $W{\cdot}m^{-1}{\cdot}K^{-1}$
θ	angle, °

Subscripts

a	ambient
al	aluminum
ce	ceramic plate
co	copper electrode
in	exhaust inlet surface
out	exhaust outlet surface
L	load resistance
n	n-type thermoelectric elements
p	p-type thermoelectric elements
t	transmission system

(*continued on next column*)

(*continued*)

$\dot{m}$	mass flow rate, $g{\cdot}s^{-1}$
n	number of fins
p	pressure, Pa
Δp	pressure drop, Pa
P	output power, W
r	radius, mm
R	electric resistance, Ω
S	seebeck coefficient, $\mu V{\cdot}K^{-1}$
T	temperature, K

1. Introduction

As a solid-state energy conversion technology, thermoelectric conversion features broad prospects in both power generation (i.e., waste heat recovery [1,2] and power sources [3,4]) and thermal management (i.e., battery [5,6], chip [7–9], and data center [10]). In the area of waste heat recovery, thermoelectric generators (TEGs) have gained

* Corresponding author.
** Corresponding author.
E-mail addresses: Ding_L@outlook.com (D. Luo), caoby@tsinghua.edu.cn (B. Cao).

https://doi.org/10.1016/j.energy.2024.131756
Received 20 February 2024; Received in revised form 20 May 2024; Accepted 22 May 2024
Available online 23 May 2024

widespread attention due to their ability to directly convert waste heat into electricity and the unparalleled merits of high reliability, compact structure, no moving parts, and a long lifespan. Initially, TEG was predominantly utilized in the aerospace industry [11]. However, with advancing research, their applications have expanded to include industrial waste heat recovery [12], automotive waste heat recovery [13,14], wearable devices [15], and wireless sensors [16] across various fields. It is not difficult to conclude that the TEG holds vast prospects in promoting clean energy and addressing energy wastage.

Despite significant progress in recent years, the TEG still faces challenges, primarily attributed to low efficiency and high costs, hindering their large-scale commercial production process [17]. The recent advances in thermoelectric studies are shown in Table 1. Currently, researchers focus on improving thermoelectric conversion efficiency in two main areas: (i) Exploring high-performance thermoelectric materials, and (ii) Optimizing the structure to increase the operating temperature difference of TEGs. The progress of nanotechnology and quantum-scale synthesis technology has resulted in the successive emergence of various new thermoelectric materials [18], including nanocomposites, nanocrystalline materials, and nanowires. These advancements have led to a significant enhancement in thermoelectric performance. Furthermore, advanced thermoelectric element structures, such as segmented design [19], two-stage design [20], and variable cross-sectional area optimized by temperature distributions [21], have been developed to enhance the performance of the TEG.

A typical TEG for automotive waste heat recovery consists of a heat sink, a heat exchanger, and thermoelectric modules (TEMs). To maximize the working temperature difference of the TEG, it is essential for the heat exchanger to efficiently absorb as much heat as possible from the exhaust gas, while simultaneously ensuring that the heat sink effectively dissipates more heat into the coolant. Due to the advantages of water cooling over air cooling and the minimal impact of coolant flow rate variations on the cold-end temperature of the TEG at a relatively high flow rate value [22], the focal point of research centers on enhancing the heat transfer efficiency of the heat exchanger. Luo et al. [23] proposed a convergent heat exchanger with a continuously decreasing flow channel cross-section along the exhaust gas direction; This innovative design led to a significant increase in both the Reynolds number and convective heat transfer coefficient along the exhaust flow direction, resulting in an augmented hot-end temperature of the TEM and an enhancement in the output performance of the TEG. Yang et al. [24] proposed a concentric annular heat exchanger, which also compresses the flow space of exhaust gas, thereby increasing the total heat transfer coefficient and improving the output performance of the TEG; Compared to traditional smooth-flow annular heat exchangers, the TEG with a concentric annular heat exchanger showed a 65 % increase in maximum net power. In addition to compressing the exhaust flow space, integrating some new configurations into the heat exchanger can also improve the heat transfer performance. Li et al. [25] proposed an annular heat exchanger with integrated heat pipes; Thanks to the incorporation of integrated heat pipes, the TEM does not need to be designed as a ring and can adapt to a curved hot-end surface. Zhao et al. [26] implemented a fluid layer between the exhaust gas and the heat exchanger, which facilitates the transfer of heat energy from the exhaust gas to TEMs through the condensation-boiling process of the medium fluid; This innovative approach significantly enhances the output performance of the TEG. Yang et al. [27] proposed a novel concentric tube-type heat exchanger that employs silicone polymer thermal conductive oil to transfer the heat from the exhaust gas; This innovative design resulted in a 15.2 % increase in the maximum output power of the new TEG compared to traditional structures.

Additionally, the insertion of flow disturbance elements into the heat exchanger proves to be an effective method for significantly enhancing heat transfer capability. Zhu et al. [28] proposed an annular TEG featuring a twisted tape and derived the optimal structural parameters through a multi-objective optimization approach; Under optimal parameters, the net power of the new TEG demonstrated a significant improvement compared to that of the TEG with a smooth channel. Li et al. [29] investigated the impact of inserting porous copper foam into the central flow area on the heat transfer performance of the heat exchanger; The findings demonstrated that, compared to the traditional TEG without porous copper foams, the utilization of porous copper foam with high porosity density and volume ratio increased the output power by 2.3 times.

In contrast to twisted tape and porous copper foam, fins offer advantages such as low cost, straightforward installation, and high efficiency, making them more widely applied. Fins can augment the heat transfer area between the heat exchanger and exhaust gas, elevate the hot-end temperature of the TEM, and consequently achieve greater output performance. Chen et al. [30] introduced a TEG featuring plate fins and conducted a performance analysis under the conditions of low-temperature waste heat recovery; The results indicated that, despite an increase in system back pressure, the TEG demonstrated significant performance improvement within the Reynolds number range of 0–1000. Yang et al. [31] implemented pin fins in an annular TEG and studied its performance through numerical simulations; They found that under the optimal design parameters, the TEG with pin fins exhibits a 5.83 % increase in output power compared to TEGs equipped with plate fins. Chen et al. [32] introduced a square pin fin and conducted a comparative study with plate fins; Their results indicated that both the installation of plate fins and square pin fins can significantly enhance the output performance of the TEG; Specifically, when the number of square pin fins reached 48, the TEG with square pin fins exhibited a higher heat-side heat transfer rate than the TEG with plate fins.

Table 1
Recent advances in thermoelectric studies.

Research object	Improvement methods	Specific implementation	Sources
TEMs	exploring high-performance thermoelectric materials	• nanocomposites	[18]
		• nanocrystalline materials	
		• nanowires	
	optimizing the structure of TEMs	• segmented design	[19]
		• two-stage design	[20]
		• variable cross-sectional area optimized by temperature distributions	[21]
Heat exchanger	compressing the exhaust flow space	• convergent heat exchanger	[23]
		• concentric annular heat exchanger	[24]
	integrating some new configurations	• heat pipes	[25]
		• fluid layer	[26]
		• silicone polymer thermal conductive oil	[27]
	inserting turbulence elements	• twisted tape	[28]
		• porous copper foam	[29]
		• plate fins	[30]
		• pin fins	[31]
		• square pin fins	[32]

However, the traditional design of fins fails to meet the requirement for temperature uniformity in the heat exchanger. Zhang et al. [33] utilized a TEG with plate fins for recovering exhaust heat and reported that the temperature of fins is the highest at the exhaust inlet and gradually decreased along the direction of exhaust flow, leading to an uneven distribution of temperature on the heat exchanger surface. Through numerical investigation, Meng et al. [34] found that the uneven surface temperature of the heat exchanger significantly deteriorates the output power of the TEM along the heat flux direction, and the maximum power output of the TEG is not enhanced but is actually reduced when too many TEMs are adopted. This power constraint stems from the cascading arrangement of TEMs. When all TEMs are connected in series, the overall output current is restricted by the minimum output current of the TEMs, while in parallel connection, the overall output voltage is constrained. Therefore, the temperature uniformity of the heat exchanger is a key factor that can not be ignored, which affects the overall output performance of the TEG, and the temperature uniformity can be improved by introducing innovative designs of the fin structure.

Additionally, to save time and costs, theoretical models have become powerful tools for predicting and optimizing TEG performance, especially when multiple parameters need to be optimized [35]. The previously published models can be categorized into: analytical models, computational fluid dynamics (CFD) models, and fluid-thermal-electric multiphysics numerical models. Among them, analytical models can quickly obtain analytical results for guiding preliminary performance analysis of TEGs. However, owing to simplifications and assumptions inherent in analytical models, the predicted results of the TEG obtained through such models inevitably deviate [36]. CFD models can be used to predict the fluid and thermal distributions in the TEG, but fail to predict electrical output performance [37]. Compared to analytical and CFD models, fluid-thermal-electric multiphysics numerical models can simultaneously calculate fluid, thermal, and electric fields while considering multiphysics coupling effects, thus achieving higher model accuracy [38]. Luo et al. [39] utilized fluid-thermal-electric multiphysics numerical models to predict the performance of a convergent TEG and completed experimental verifications; Their study showed that the maximum deviation between numerical results and experimental results is approximately 2.4 %, exhibiting a high accuracy of the multiphysics numerical model.

As mentioned above, the design of fins plays a crucial role in facilitating the heat exchanger to absorb more heat from the exhaust gas while maintaining uniformity in the temperature across the heat exchanger surface. To realize this objective, the present work introduces a diverging fin, which is integrated into a hexagonal TEG with a circular channel. Diverging fins differ from traditional fins in a key aspect: their cross-sectional area continuously increases along the direction of exhaust gas flow, which enhances the heat transfer performance downstream of the exhaust gas, thereby improving the temperature uniformity of the heat exchanger. However, the diverging design of fins also results in additional pressure drop. It is imperative to strike a balance between heat transfer efficiency and pressure drop to avoid an undue increase in engine pumping power [40]. Kim et al. [41] conducted experiments and demonstrated that, under the eight most common driving conditions of a car, the acceptable pressure drop for the hexagonal TEG is 2.1 kPa. Hence, in this study, the maximum allowable pressure drop for the heat exchanger is established at 2.1 kPa, guiding the design of the hexagonal TEG with diverging fins towards the goal of maximizing output power. The key research procedures of this paper are delineated as: (i) Developing a fluid-thermal-electric multiphysics numerical model for the hexagonal TEG and validating its accuracy; (ii) Utilizing the established numerical model to conduct a comprehensive analysis and comparison of the performance between diverging fins and traditional fins; (iii) Within the limitation of a maximum pressure drop of 2.1 kPa, optimizing the diverging angle, quantity, and height of diverging fins to maximize the output power.

The paper is organized as follows: Section 2 outlines the structure of the hexagonal TEG and the design of diverging fins; Section 3 introduces and validates the numerical model; Section 4 presents a comprehensive optimization for the hexagonal TEG with integrated diverging fins, aiming to achieve maximum output power; Finally, Section 5 provides a summary of the conclusions.

2. Structure of the hexagonal TEG

The proposed hexagonal TEG is composed of 6 S-shaped liquid cooling heat sinks, 30 TEMs and a hexagonal heat exchanger with diverging fins, as shown in Fig. 1. The hexagonal heat exchanger is configured with a circular exhaust flow channel, with a diameter of 50 mm, to match the pipeline diameter of most automobile exhaust pipes, thereby contributing to the mitigation of pressure drops induced by the TEG. A hollow cylindrical tube with a radius of r is placed inside the heat exchanger to secure diverging fins. Simultaneously, the introduction of diverging fins increases the contact area between exhaust gas and heat exchanger, thereby enhancing the convective heat transfer and improving the hot-side temperature of TEMs. Also, two semispherical protrusions are applied on both sides of the hollow cylindrical tube to facilitate the uniform and smooth flow of automotive exhaust gas throughout the entire fin area. Here, the width of the hot-side surface of the hexagonal heat exchanger is 32 mm. Accordingly, the TEM with dimensions of 30 mm × 30 mm × 3.4 mm (L × W × H) is adopted in this work. Each hot-side surface of the hexagonal heat exchanger is uniformly equipped with 5 TEMs, with each TEM composed of 72 pairs of p-type and n-type thermoelectric elements, 144 copper electrodes, and two ceramic plates. To ensure the accuracy of theoretical analysis, the temperature-dependent thermoelectric properties are taken into account, with detailed parameters of the TEM listed in Table 2 [42], where the maximum error of the fitting function is within 1 %, and the range of T is from 300 K to 550 K. On the cold side of TEMs, a heat sink with a thickness of 5 mm is employed to dissipate its heat. Inside the heat sink, there is an S-shaped channel with a diameter of $D = 4$ mm to ensure its cooling performance. The heat sink and hexagonal heat exchanger feature the same length and are both made of aluminum materials. Furthermore, air is used to replace the exhaust gas, while cooling water serves as the medium for heat dissipation.

Details of the internal diverging fins in the heat exchanger are given in Fig. 2. Along the direction of exhaust gas flow, the cross-sectional area of the diverging fins continuously increases, as can be seen in Fig. 2(a). This design effectively enhances the heat transfer between exhaust gas and heat exchanger, especially in the downward flow direction, thereby improving the uniformity of the hot-side temperature of the TEMs and enhancing the electrical output. Fig. 2(b) illustrates the axial cross section of the diverging fins. Here, the diverging angle, α, is defined as the angle between the long edge of the fin and the axial direction. The output performance of the proposed hexagonal TEG is sensitive to this diverging angle, and it will be optimized in the following sections. Fig. 2 (c) shows the radial cross section of the diverging fins at the exhaust gas inlet, where the central angle of fins is fixed at $\theta = 2.5°$. The height of the diverging fins is defined as h, and the radius r of the hollow cylindrical tube varies with h, with the relationship being: $r + h = 25$ mm. Considering that the diverging angle (α), height (h), and number of diverging fins (n) interact with each other, a comprehensive optimization is carried out on these three parameters to maximize the output performance of the hexagonal TEG.

3. Numerical model

To predict and guide the optimization of the TEG performance, a fluid-thermal-electric multiphysics numerical model for the hexagonal TEG is developed. Also, the finite element method is adopted to solve the numerical model via the commercial software of COMSOL Multiphysics. Details for the numerical model are introduced below.

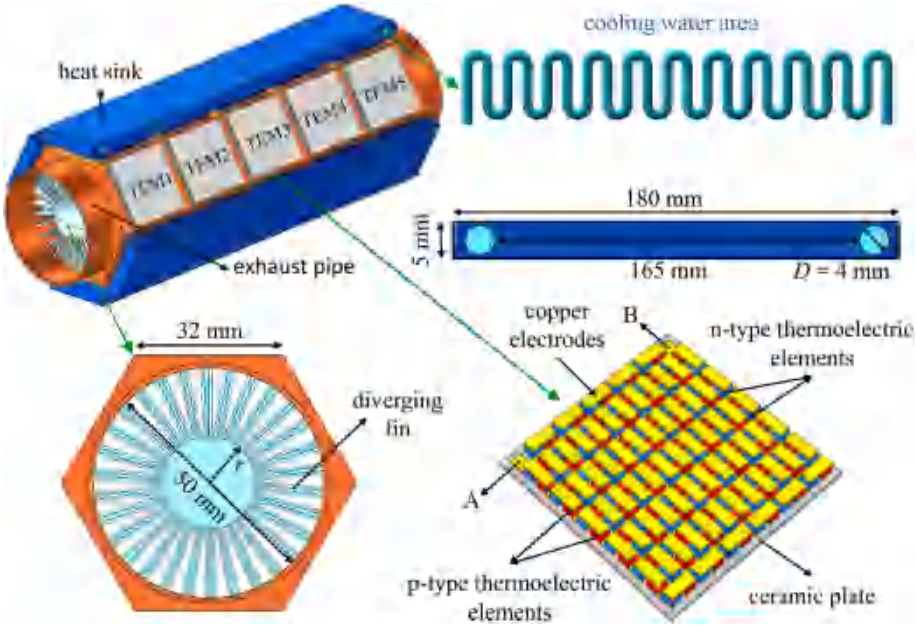

Fig. 1. Schematic diagram of the hexagonal TEG.

Table 2
Geometric dimensions and material parameters of TEM.

Parameter	p-type thermoelectric element	n-type thermoelectric element	Ceramic plates	Copper electrodes
Dimensions (L × W × H mm^3)	1.8 × 1.8 × 1.2	1.8 × 1.8 × 1.2	30 × 30 × 0.8	4.1 × 1.8 × 0.3
Thermal conductivity ($W{\cdot}m^{-1}{\cdot}K^{-1}$)	$1.8022\times10^{-10}T^4$-$2.8631\times10^{-7}T^3$ + $1.7941\times10^{-4}T^2$-$0.052T$ + 6.8208	$-1.0257\times10^{-9}T^4$ + $1.6523\times10^{-6}T^3$ -$9.6842\times10^{-4}T^2$ + $0.2447T$-21.5585	22	400
Electrical resistivity ($10^{-5}\Omega{\cdot}$ m)	$-6.839\times10^{-10}T^4$ + $9.9566\times10^{-7}T^3$ -$5.3215\times10^{-4}T^2$ + $0.1298T$-11.506	$4.3486\times10^{-10}T^4$-$8.9267\times10^{-7}T^3$ + $6.4322\times10^{-4}T^2$-$0.192T$ + 21.419	–	1.67×10^{-3}
Seebeck coefficient ($\mu V{\cdot}K^{-1}$)	$1.9359\times10^{-8}T^4$-$3.7183\times10^{-5}T^3$ + $2.4243\times10^{-2}T^2$-$6.366T$ + 772.02	$1.1468\times10^{-8}T^4$-$1.2129\times10^{-5}T^3$ + $3.5018\times10^{-3}T^2$-$0.1535T$-189.21	–	–

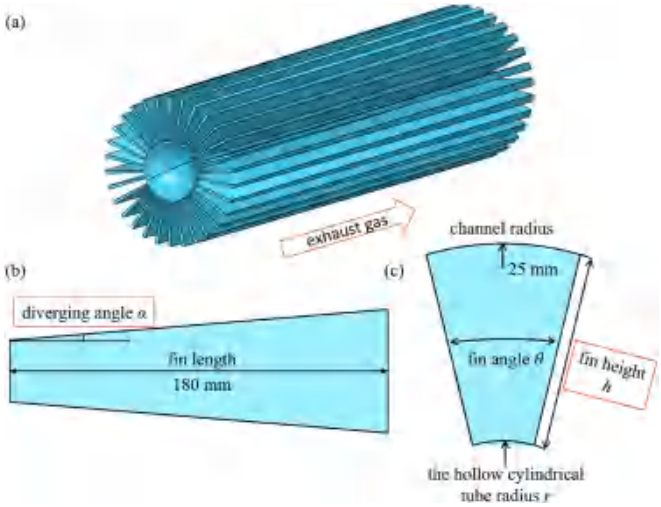

Fig. 2. Schematic diagram of the diverging fins. (a) 3D Architecture diagram; (b) Axial cross section; (c) Radial cross section at the exhaust inlet.

3.1. Governing equations

Fig. 3 depicts a schematic diagram of the governing equations of the numerical model. The basic equations of the numerical model consist of conservation equations for fluid, thermal, and electrical fields. Both exhaust gas and cooling water are considered as incompressible fluids, following the mass, momentum, and energy conservation principles [43]. Also, a standard k - ε turbulence model is applied to calculate the fluid dissipation rates and kinetic energy [44]. The hexagonal heat exchanger, heat sinks, as well as ceramic plates, only involve heat transfer and follow the energy conservation equation. The thermoelectric elements and copper electrodes involve heat and current transfer, adhering to the conservation of electrical and thermal fields [45]. The coupling of thermal and electrical fields occurs in the regions of thermoelectric elements and copper electrodes. For example, as the current flows through TEMs, Joule heat is generated in copper electrodes and thermoelectric components, and in thermoelectric elements, due to the thermoelectric effects, Peltier heat and Thomson heat are also accompanied. These parasitic heats are treated as energy source terms in the conservation equations [46]. Further details for this model can be found in Ref. [47].

3.2. Boundary conditions

Fig. 4 displays the finite element model and its boundary conditions for the hexagonal TEG. Considering the computational cost and symmetrical structure, the finite element model is established using a 1/6 geometry of the hexagonal TEG. Accordingly, symmetric boundary conditions are applied on these symmetrical surfaces. In fluid domains, boundary conditions for temperature and flow velocity are specified at the inlet surface of the cooling water channel, temperature and mass flow rate conditions are defined on the inlet surface of the exhaust channel, and pressure boundary conditions are defined on the outlet surfaces of both exhaust and cooling water channels. In the computing

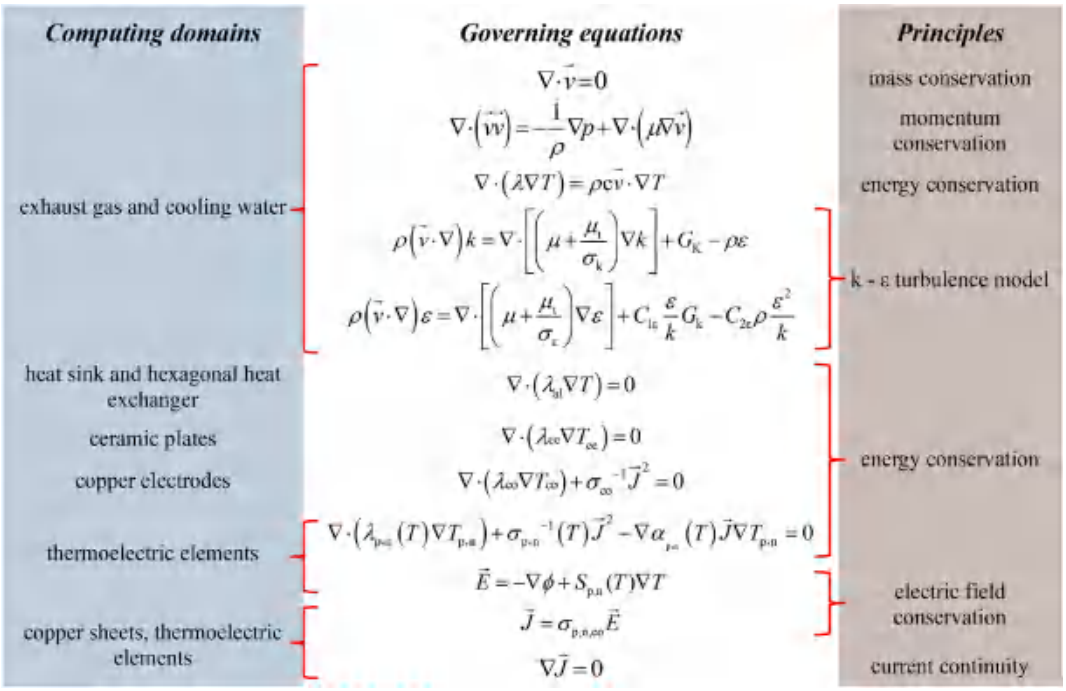

Fig. 3. Basic theory of the fluid-thermal-electric multiphysics numerical model.

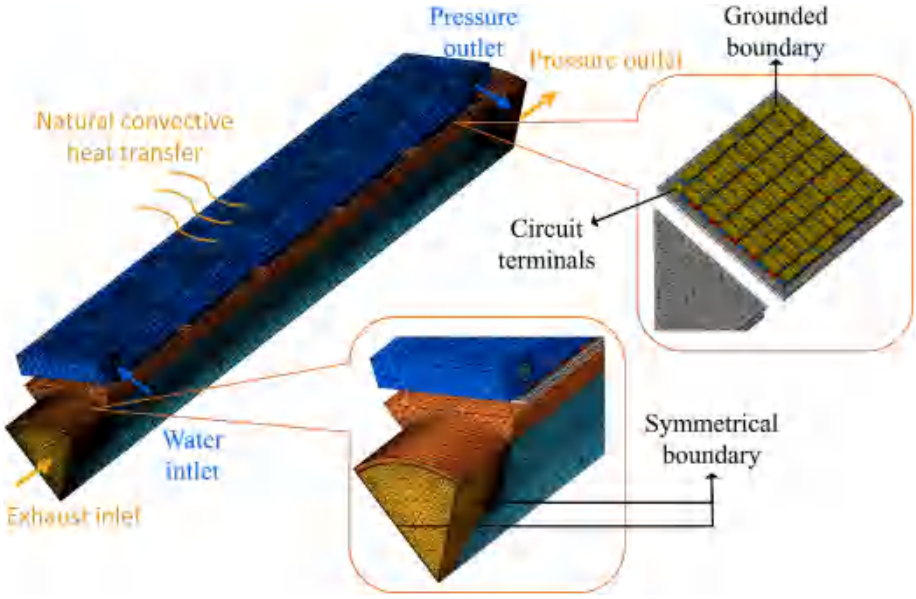

Fig. 4. Finite element model and boundary conditions of the hexagonal TEG.

domain of the electrical field, the surface B of the TEM closing to the exhaust inlet, as marked in Fig. 1, is defined as the grounded boundary, while the remaining surfaces A and B are designated as circuit terminals. Besides, virtual circuits are introduced to ensure TEMs are connected in series, and an additional circuit with an external resistance R_L is introduced to form a loop between TEMs and load resistance. On the surfaces of the TEG exposed to the external environment, a convective heat transfer boundary condition is defined, as follows:

$$\lambda\frac{\partial T}{\partial n}=h_{\alpha}(T-T_{\alpha}) \tag{1}$$

with h_a and T_a being the ambient convection heat transfer coefficient and ambient temperature respectively. Specific values for different boundary conditions can be found in Table 3. It is worth noting that, due to the adoption of a 1/6 geometric model, the mass flow rate in the model should be divided by 6.

3.3. Parameter definition

The TEMs convert the absorbed heat into electricity due to the Seebeck effect. Due to the use of a 1/6 model, the output power of the entire hexagonal TEG is equal to 6 times the obtained value, defined as follows:

$$P_{\text{out}}=\frac{6{U_{\text{out}}}^2}{R_L} \tag{2}$$

where, U_{out} is the output voltage of the 1/6 structure, and R_L is the

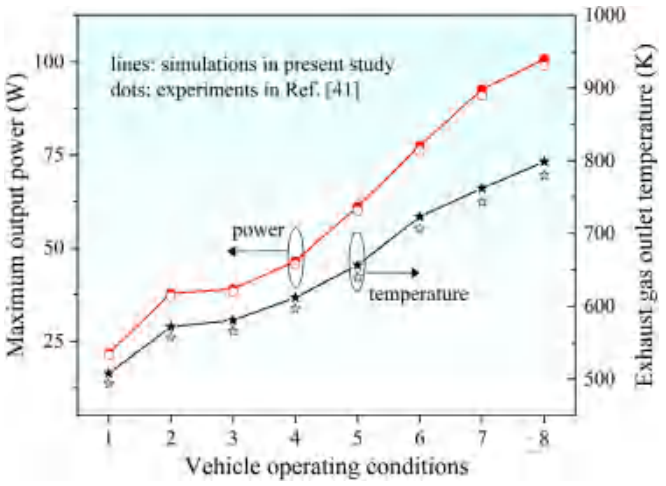

Fig. 5. Comparison between experiments in Ref. [41] and simulations of in present study.

Table 3
Boundary conditions of the fluid-thermal-electric multiphysics numerical model for the hexagonal TEG.

Computing domain	Boundary	Value	Unit
Cooling water	temperature inlet	300	K
	velocity inlet	1	m/s
	pressure outlet	standard atmospheric pressure	Pa
Exhaust gas	temperature inlet	from 350 to 550 at every 50	K
	mass flow rate inlet	from 10 to 60 at every 5	g/s
	pressure outlet	standard atmospheric pressure	Pa
Surface B of the first TEM	grounded	0	V
The remaining surfaces A and B	circuit terminals	NA	NA
Heat loss	ambient heat transfer coefficient	15	$W/(m^2 \cdot K)$
	ambient temperature	300	K
Symmetrical surfaces	symmetric boundary	NA	NA

external load.

In addition, the introduction of diverging fins can not only enhance the heat transfer but also generate additional pressure drop. According to Ref. [41], the pressure drop cannot exceed the allowable value of 2.1 kPa for the use of TEG in the exhaust system. Therefore, the pressure drop should be considered during optimizations, which can be expressed as:

$$\Delta p = p_{in} - p_{out} \tag{3}$$

where p_{in} and p_{out} are respectively the average pressure on the inlet and outlet surfaces of the exhaust exchannel.

3.4. Cell independence validation

Before conducting extensive numerical calculations, cell independence validation is required because coarse cells may lead to deviations in simulation results, while overly fine cells may increase computational costs. To select a suitable cell system, the output power of the TEG was compared under five cell systems, as shown in Table 4. Here, simulations were conducted with boundary conditions of $T_{in} = 550$ K and $R_L = 5$ Ω,

Table 4
Output power and its deviation of the TEG under different cell systems.

Cell system	Cell number	Output power with $\dot{m} = 20$ g/s	Output power with $\dot{m} = 40$ g/s	Output power with $\dot{m} = 60$ g/s	Deviation
Cell I	4620768	95.3727 W	145.8608 W	172.0233 W	NA
Cell II	2111782	95.3727 W	145.8608 W	172.0233 W	0 %
Cell III	1095726	95.3765 W	145.8666 W	172.0302 W	0.004 %
Cell IV	536527	95.3908 W	145.8884 W	172.0560 W	0.015 %
Cell V	196543	95.4137 W	145.9234 W	172.0973 W	0.024 %

because the maximum output power of the 1/6 TEG occurs when $R_L = 5$ Ω through a preliminary analysis of load response characteristics. It can be observed that with the increase in the number of cells, the output power slightly decreases. When the cell number reaches 1095726 the output power remains essentially constant. To balance model accuracy and computation costs, Cell III was chosen for numerical simulations under different parameters in this work.

3.5. Experimental validation

In Ref. [41], Kim et al. conducted experimental studies on a finned hexagonal TEG under 8 common vehicle operating conditions. To validate the accuracy of the used numerical model, a 1/6 geometric model of the hexagonal TEG used in Ref. [41] was established, and the model developed in this work was used for simulations. The simulation conditions used are consistent with those in Ref. [41], with the coolant mass flow rate of 27 g/s and exhaust conditions in Table 5. Fig. 5 shows the comparison between numerical simulation and experimental results under different vehicle operating conditions. It can be observed that both the exhaust outlet temperature and the maximum output power of the TEG obtained from the fluid-thermal-electric multiphysics numerical model are slightly higher than the experimental results. This deviation is attributed to the neglect of thermal grease in the numerical model. The maximum temperature deviation is approximately 2.75 %, and the maximum power deviation is about 1.94 %, which is within an acceptable range. In summary, the results obtained align well with the literature, confirming the feasibility of the model.

4. Results and discussion

4.1. Numerical results

Fig. 6 illustrates the physical field distribution characteristics of a 1/6 hexagonal TEG with traditional fins. The parameters of the traditional fins are: $\alpha = 0°$, $n = 30$, $h = 15$ mm. The inlet temperature T_{in} of the exhaust gas is 550 K, and the mass flow rate $\dot{m}$ is 30 g/s. The temperature along the heat exchanger's surface experiences a notable decrease in the direction of the exhaust flow, as depicted in Fig. 6(a). This occurrence is mainly attributed to the heat dissipation by cooling water. Additionally, from a side view, it is evident that the temperature drop of the fins mainly occurs axially, with the highest temperature at the entrance of

Table 5
Correspondence between vehicle operating conditions and exhaust gas conditions.

Vehicle operating conditions	Exhaust gas mass flow rate (g/s)	Exhaust gas inlet temperature (K)
1	16.33	590.26
2	18.83	656.67
3	20.36	664.71
4	22.22	694.65
5	24.03	743.81
6	27.11	811.56
7	32.22	847.46
8	37.39	886.01

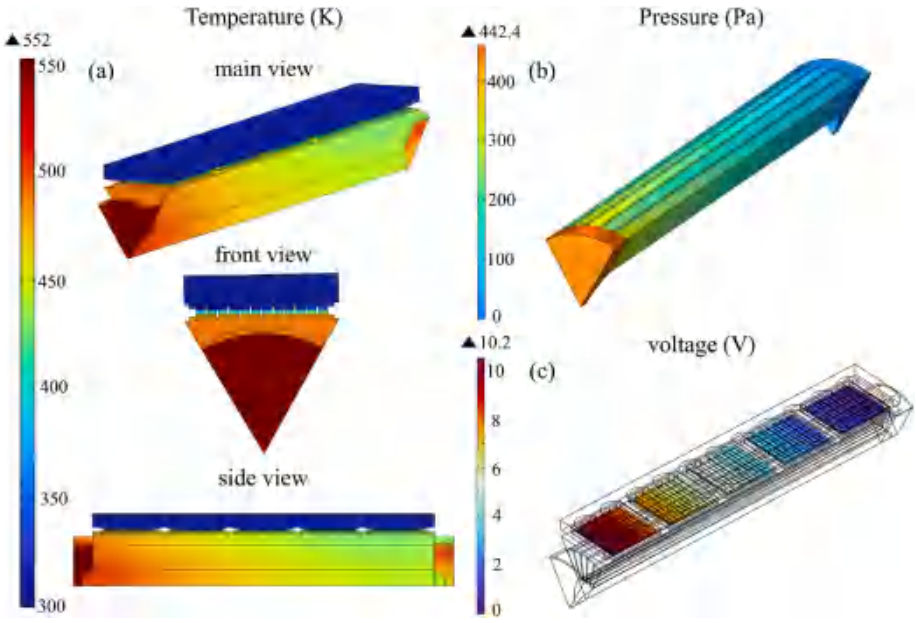

Fig. 6. Numerical results of the hexagonal TEG. (a) Temperature distributions; (b) Pressure distributions; (c) Voltage distributions.

the exhaust gas and gradually decreasing along the direction of the exhaust flow. This temperature drop leads to a corresponding decrease in the output of TEMs, and additional electrical energy loss also occurs when TEMs are connected to each other, especially in the traditional all series topology connection. Therefore, a novel design of diverging fins is introduced in the heat exchanger to address this issue, wherein the diverging fins enable enhancing the heat transfer between exhaust gas and heat exchanger, especially in the downward flow direction. Fig. 6(b) shows the pressure distribution of the exhaust. By extracting the average pressure on the inlet and outlet surfaces of the exhaust channel, the exhaust pressure drop of the entire TEG can be obtained. In the traditional structure, the pressure drop is 442.4 Pa at the mass flow rate of 30 g/s, which is far below the allowable value of 2.1 kPa, and thus the heat transfer performance of the heat exchanger can be further improved by introducing some enhanced heat transfer methods. Fig. 6(c) displays the voltage distribution of TEMs in a 1/6 hexagonal TEG. In this study, five TEMs are connected in series, and the output performance of the hexagonal TEG is constrained by the minimum current within the TEMs [48]. The novel diverging fins proposed in this study offer a solution to this performance constraint, leading to an improvement in the overall output performance of the hexagonal TEG.

4.2. Comparison between traditional fins and diverging fins

To analyze the mechanism by which diverging fins improve the heat transfer performance, a comparison with traditional fins is conducted in this section. As shown in Fig. 7, Fig. 7(a) represents a hexagonal TEG with traditional fins, and Fig. 7(b) shows a hexagonal TEG with diverging fins used for comparison. The parameters of the diverging fins are: $\alpha = 0.2°$, $n = 30$, $h = 15$ mm. The traditional fins and diverging fins used for comparison have the same quantity and height. Additionally, both configurations are designed with the same boundary conditions: $T_{in} = 550$ K, $\dot{m} = 30$ g/s.

Fig. 8(a) shows the exhaust velocity distributions of the hexagonal TEG with different fins. Obviously, compared to traditional fins, the diverging fins enable a higher flow velocity within the heat exchanger due to the smaller cross-sectional area in the flow channels, especially in the downward flow direction. Additionally, the higher the flow velocity is, the greater the convective heat transfer coefficient will be. The cross-sectional area of the exhaust channel in the heat exchanger with diverging fins continuously decreases along the heat flux direction, resulting in the continuous increase of the convective heat transfer coefficient. This helps mitigate the adverse effects of exhaust temperature drop and improves the thermal performance and temperature

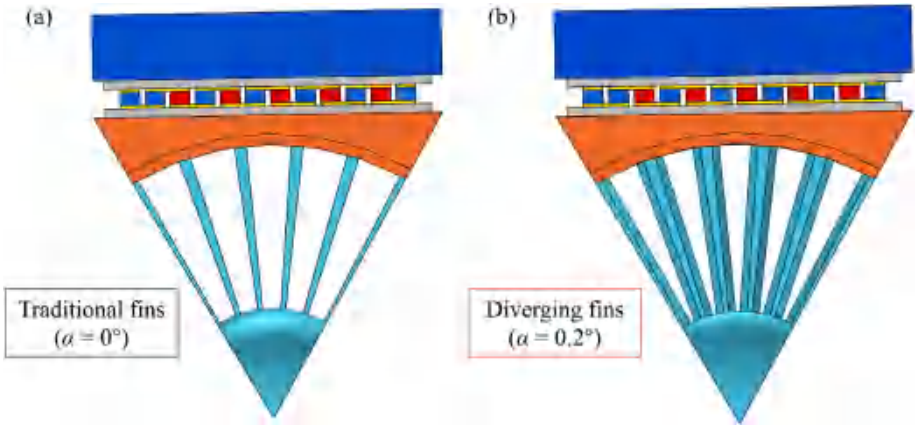

Fig. 7. Schematic diagram of the hexagonal TEG with different fins. (a) Traditional fins; (b) Diverging fins.

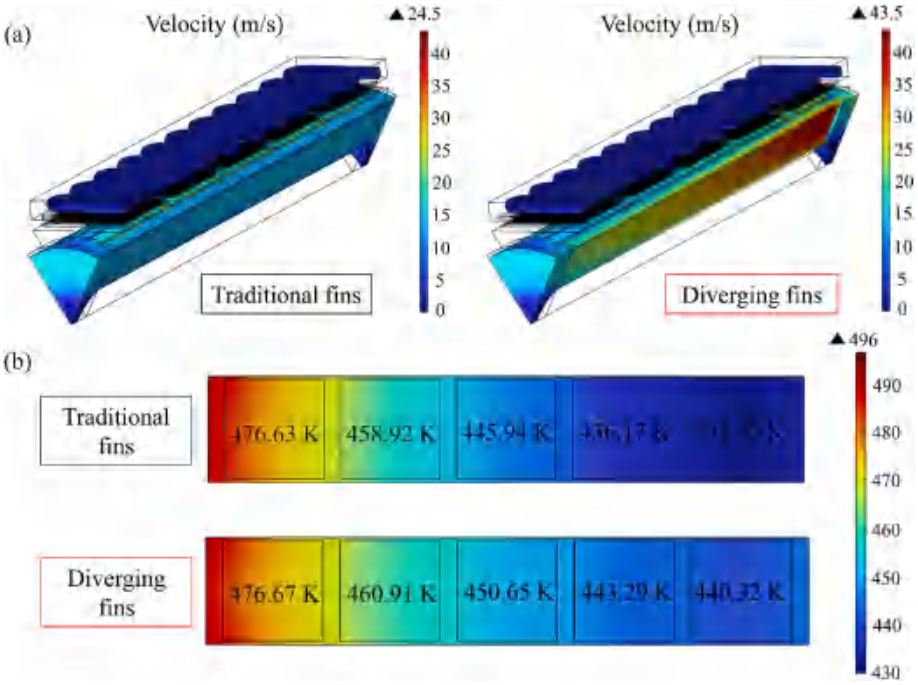

Fig. 8. Physical field distribution characteristics of the hexagonal TEG with different fins. (a) Velocity distributions; (b) Temperature distributions on the hot-side surface of the heat exchanger.

uniformity of the heat exchanger. However, the diverging design of the fins inevitably increases the pressure drop. Therefore, in order to balance the pressure drop and heat transfer performance, a comprehensive optimization for the diverging angle α, number of fins n, and fin height h of the diverging fins is conducted in Section 4.3, ensuring that the pressure drop remains within a reasonable range.

Fig. 8(b) shows the temperature distributions on the hot-side surface of the heat exchanger, with the average surface temperature data at the hot end for each TEM. Compared to traditional fins, the use of diverging fins leads to a higher and more uniform temperature distribution on the hot side of the heat exchanger. In the heat exchanger with traditional fins, the cross-sectional area of the exhaust channel remains unchanged, and the heat exchanger suffers from the exhaust temperature drop, resulting in lower temperature uniformity on the hot side surface [49]. As can be observed, the hot-side temperature of the last TEM experiences an increase of 8.92 K when applying the diverging fins, which will lead to a corresponding increase in the output power of the hexagonal TEG. Besides, the TEG with diverging fins benefits from improved temperature uniformity, resulting in a less electrical energy loss when TEMs are connected in series. Consequently, the use of diverging fins can not only improve the output power but also lower the power loss, which is an effective optimization approach for traditional fin structures.

4.3. Exploration of optimal fin parameters

Reasonable structural design can further enhance the gain effect of diverging fins. Therefore, the fins parameters, including diverging angle α, number of fins n, and fin height h, are optimized in this section. To maximize the output performance of the hexagonal TEG, the selection of fin parameters for diverging fins should meet the following criteria:

1) The overall pressure drop of the hexagonal TEG should be below 2.1 kPa [41];
2) Maximize the output power.

4.3.1. Effect of the diverging angle

The influence of different diverging angles α on the output performance of the hexagonal TEG is investigated in this subsection, while fixing the fin height h and the number of fins n as 15 mm and 30 respectively. Due to the structure limitations, four cases of diverging angle were considered with $\alpha = 0.05°$, $\alpha = 0.1°$, $\alpha = 0.15°$, and $\alpha = 0.2°$. Fig. 9(a) shows the output power of the hexagonal TEG with different α as a function of exhaust temperatures. The findings reveal a rapid increase in the output power of the hexagonal TEG with rising temperatures. The increased exhaust temperature leads to a larger temperature gradient across TEMs, thus increasing the output power of the TEG. Furthermore, the disparity in output power between the hexagonal TEG equipped with diverging fins and traditional fins consistently widens. The gain of diverging fins increases with a larger diverging angle, and this effect is more pronounced at higher exhaust temperatures. At the same time, the increase in the diverging angle α leads to a larger pressure drop, as shown in Fig. 9(b). With the increase in exhaust inlet temperature, the pressure drop slightly increases, because of the temperature dependence of air density. Considering that the influence of exhaust temperature on pressure drop is tiny, and the temperature changes only affect the amplitude of output power, without affecting the optimization results of fin parameters, the influence of exhaust temperature is neglected in the following sections.

Fig. 10(a) shows the output power of the hexagonal TEG with different α as a function of exhaust mass flow rate. The output power of the hexagonal TEG increases with the increase in exhaust mass flow rate. In addition, compared to traditional fins, the hexagonal TEG with diverging fins always features a higher output power. With the increase in α, the gain of diverging fins becomes more pronounced. For example, at a mass flow rate of 35 g/s, as the diverging angle increases from 0.05° to 0.2°, the power improvement increases from 0.68 % to 5.38 %. This is attributed to the fact that under the same mass flow rate, the larger the diverging angle of fins, the faster the flow velocity in the downstream direction of the exhaust gas, resulting in a higher heat transfer coefficient. At the same time, larger mass flow rates result in larger pressure drops, as shown in Fig. 10(b). When the exhaust mass flow rate increases to a certain value, the pressure drop of the hexagonal TEG with $\alpha = 0.1°$,

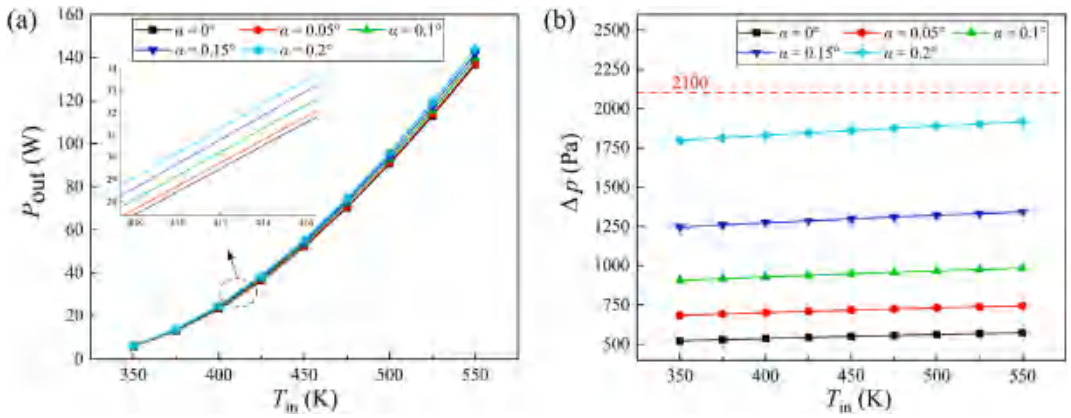

Fig. 9. Output performance of the hexagonal TEG with different α as a function of exhaust temperature. (a) Total output power; (b) Pressure drop. (e.g. $\dot{m} = 35$ g/s).

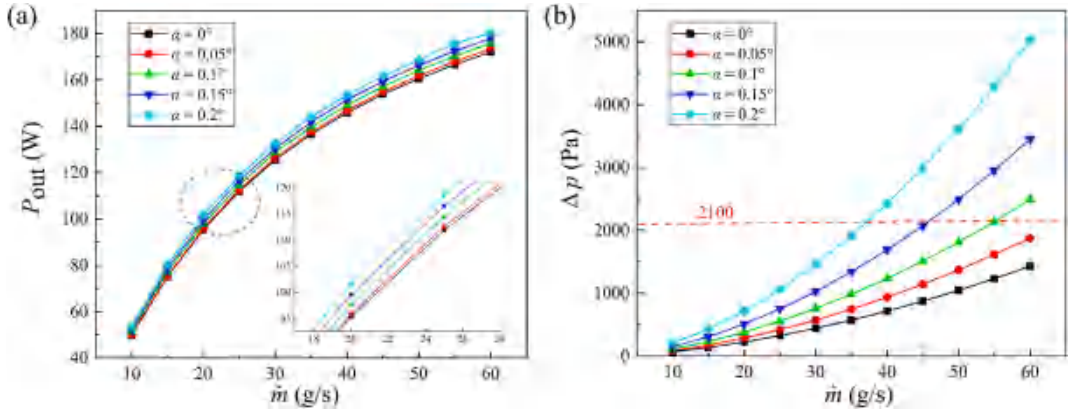

Fig. 10. Output performance of the hexagonal TEG with different α as a function of mass flow rate. (a) Total output power; (b) Pressure drop. (e.g. $T_{in} = 550$ K).

$\alpha = 0.15°$, and $\alpha = 0.2°$ exceeds the acceptable pressure drop of 2.1 kPa. Therefore, the range of exhaust mass flow rate determines the optimal value of α for diverging fins. For example, within the mass flow rate range of 0–35 g/s, $\alpha = 0.2°$ is suggested.

Through the above analysis, it is known that increasing the diverging angle α of diverging fins can always enhance the output power of the hexagonal TEG, but it also causes an additional pressure drop. The pressure drop is greatly influenced by the exhaust mass flow rate, and thus the appropriate α should be determined according to the displacement of vehicles. Additionally, the exhaust temperature has a relatively small impact on the pressure drop, therefore, the increase of exhaust temperature can improve the output performance of the hexagonal TEG without affecting the pressure drop.

4.3.2. *Effect of the number of fins*

The effect of the number of fins n on the output performance of the

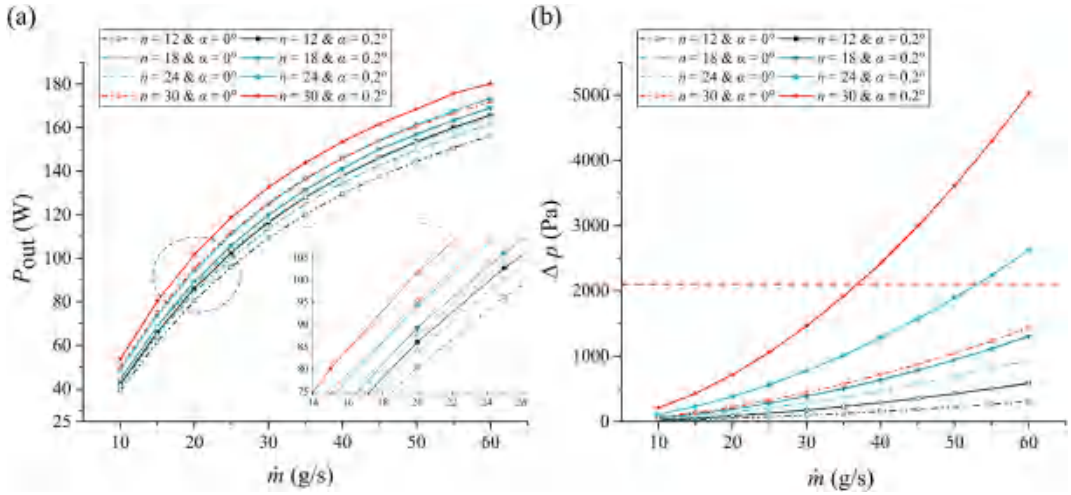

Fig. 11. Comparison of output performance between diverging fins and traditional fins with different n under different mass flow rates. (a) Total output power; (b) Pressure drop (e.g. $T_{in} = 550$ K).

hexagonal TEG is investigated in this subsection, while fixing the diverging angle α and fin height h as 0.2° and 15 mm respectively. Also, a comparison between the diverging fins and traditional structure (α = 0°) is conducted. Fig. 11(a) shows a comparison of output power between diverging fins and traditional fins with different n under different mass flow rates. The output power of the hexagonal TEG increases with the increase in the number of fins. It can be observed that both the number of fins and the diverging angle have a significant influence on the output power. For example, the output power of the hexagonal TEG with $\alpha = 0.2°$ and $n = 24$ approaches that with $\alpha = 0°$ and $n = 30$. Also, when $\alpha = 0°$ and $\dot{m} = 10$ g/s, as the number of fins increases from 12 to 30, the output power increases by 26.87 %. This is attributed to the significant increase in the number of fins, which greatly increases the heat transfer area between the exhaust gas and heat exchanger, resulting in a significant improvement in the heat absorption capacity of the heat exchanger. Additionally, it is observed that when $n = 30$ and $\dot{m} = 10$ g/s, as the diverging angle increases from 0° to 0.2°, the output power only increases by 7.47 %. Consequently, compared to the diverging angle, the number of fins has a more significant impact on the output power of the hexagonal TEG. The variation in pressure drop is shown in Fig. 11(b). An increase in the number of fins leads to a higher pressure drop. Combined with Fig. 10(b), it can be obtained that, both the diverging angle and the number of fins significantly affect the pressure drop. It can be concluded that, to maximize the output power, the optimization of the number of fins takes precedence over the optimization of diverging angle. Therefore, the number of fins ($n = 30$) is suggested.

4.3.3. Effect of the fin height

This subsection explores the influence of fin height h on the output performance of the hexagonal TEG, with a fixed diverging angle α of 0.2° and the number of fins n of 30. Fig. 12(a) shows a comparison of output power between diverging fins and traditional fins with different h under different mass flow rates. Obviously, the output power of the hexagonal TEG exhibits an augmentation with the increase in fin height. This phenomenon can be attributed to the enlarged heat transfer area between the heat exchanger and exhaust, consequently enhancing the hot-side temperature of TEMs. Also, when $\alpha = 0°$ and $\dot{m} = 10$ g/s, as the fin height increases from 7.5 mm to 15 mm, the output power increases by 5.2 %. The effect of fin height on the output power of the hexagonal TEG is comparatively insignificant, standing in contrast to the 7.47 % increment of the diverging angle (from $\alpha = 0°$ to $\alpha = 0.2°$) and the 26.87 % increment of the number of fins (from 12 to 30). Besides, a notable reduction in pressure drop caused by the heat exchanger is evident with the increase in fin height, as depicted in Fig. 12(b). As the fin height decreases, the hollow cylindrical tube occupies more space in the exhaust channel, and the cross-sectional area of the exhaust channel is smaller, resulting in greater flow resistance. Combined with Figs. 10(b) and Fig. 11(b), the influence of fin height on pressure drop is greater than that of diverging angle and number of fins. From the above analysis, it can be deduced that an increased fin height consistently yields a positive impact on the performance of the hexagonal TEG, enabling a higher output power and a lower pressure drop. Moreover, the influence of fin height on the output power of the hexagonal TEG is relatively smaller than that of the number of fins and diverging angle. Hence, to maximize the performance of the hexagonal TEG, the fin height of h = 15 mm is suggested.

4.4. Selection of the optimal fin parameters under different conditions

The above analysis suggests that, in terms of output power, the number of fins has the most pronounced effect, followed by the diverging angle, and lastly, the fin height. Regarding pressure drop, the fin height exerts the most substantial impact, followed by the diverging angle and the number of fins. To maximize the performance of the hexagonal TEG, the number and height of fins should be as large as possible within the acceptable structural limits. In this study, optimal values for the fin height and the number of fins are h = 15 mm and n = 30, respectively. Regarding the crucial parameter of the diverging angle, it is closely related to pressure drop. It necessitates a flexible selection of a suitable α value based on the range of exhaust mass flow rates. Within the limit of the maximum acceptable pressure drop of 2.1 kPa for the hexagonal TEG [41], the optimal α values are determined according to the different exhaust flow rates, as listed in Table 6.

It can be observed that, when the exhaust mass flow rate is lower

Table 6
Optimal α values under different maximum exhaust flow rates.

Maximum mass flow rate	Optimal α	Max Δp	Max P_{out}	Improvement of P_{out} compared to traditional fins
35 g/s	0.2°	1915.82 Pa	143.94 W	5.83 %
45 g/s	0.15°	2074.99 Pa	159.36 W	3.58 %
55 g/s	0.1°	2097.57 Pa	170.27 W	2.20 %
60 g/s	0.05°	1874.09 Pa	173.46 W	0.84 %

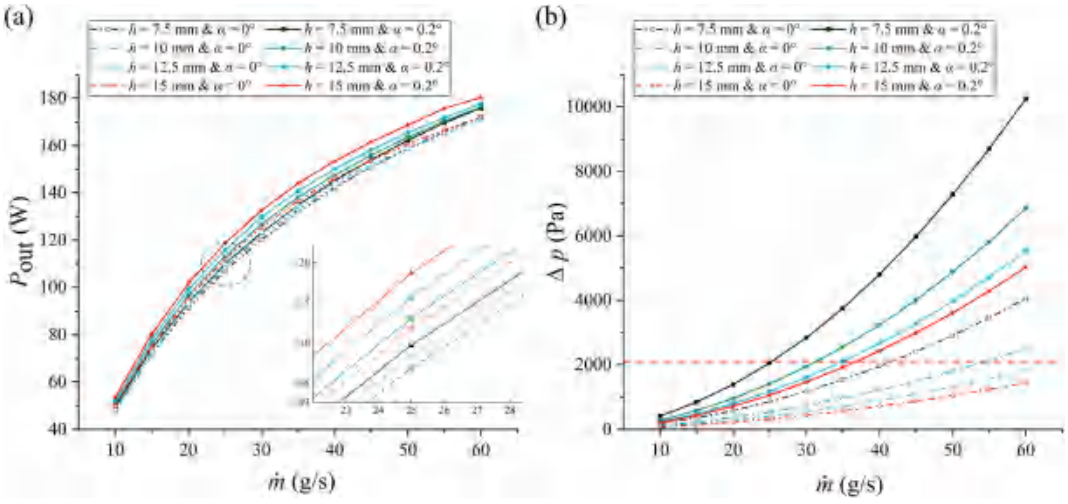

Fig. 12. Comparison of output performance between diverging fins and traditional fins with different h under different mass flow rates. (a) Total output power; (b) Pressure drop (e.g. T_{in} = 550 K).

than 35 g/s, the optimal value of the diverging angle can be set to the structural limit, which is 0.2°. However, when the mass flow rate is higher, the diverging angle should be correspondingly reduced to ensure that the pressure drop does not exceed the allowable value. Fig. 13 demonstrates the effect of mass flow rate on the performance gains under the optimal $\alpha = 0.2°$. As the mass flow rate increases from 10 g/s to 35 g/s, the power improvement decreases from 7.47 % to 5.83 %. It seems that as the mass flow rate decreases, the gains introduced by the diverging fins become more pronounced.

5. Conclusions

In order to improve the heat transfer and temperature uniformity of the heat exchanger, and consequently enhance the output performance of the hexagonal TEG. In this work, a novel design of diverging fins is proposed, and the difference compared to traditional fins lies in the continuous increase of their cross-sectional area along the heat flux direction. Then, a fluid-thermal-electric multiphysics numerical model of 1/6 hexagonal TEG is established to predict its output performance under various parameters. Finally, the key structural parameters of the diverging fin, including diverging angle, number of fins, and fin height, are optimized through numerical simulations. The principal conclusions are as follows:

(1) The proposed novel design of diverging fins can improve the heat transfer performance and temperature uniformity of the heat exchanger, enhancing not only the output power of the hexagonal TEG but also reducing the electrical power loss caused by the series connection among TEMs, which is an effective optimization method for traditional fin-based heat exchanger.
(2) As the diverging angle, number, and height of fins increase, both output power and pressure drop of the hexagonal TEG continuously increase, except for the pressure drop which decreases with the increase of fin height. In terms of output power, the number of fins has the most pronounced effect, followed by the diverging angle, and lastly, the fin height. Regarding pressure drop, the fin height exerts the most substantial impact, followed by the diverging angle and the number of fins.
(3) Through numerical optimizations, the optimal values of 30 and 15 mm for the number of fins and fin height are obtained. While the optimal diverging angle is related to the exhaust mass flow rate due to the limite of allowable pressure drop. When the exhaust mass flow rate is lower than 35 g/s, the optimal value of the diverging angle is 0.2°, and with the increase of flow rate, the optimal diverging angle decreases correspondingly.
(4) The optimized hexagonal TEG with diverging fins can reach an output power of 143.94 W at the exhaust mass flow rate of 35 g/s and temperature of 550 K, which is 5.83 % higher than that of the traditional structure. Meanwhile, the pressure drop is only 1.92 kPa, within the allowable limit for the hexagonal TEG. Besides, as the mass flow rate decreases, the gains introduced by the diverging fins become more pronounced.
(5) The current study focuses on the optimization for individual fin parameters. However, the diverging angle, number, and height of the diverging fins interact with each other. In order to obtain more comprehensive optimization results, a multi-objective optimization algorithm will be introduced in future work to simultaneously optimize these parameters.

CRediT authorship contribution statement

Ding Luo: Writing – original draft, Supervision, Methodology, Conceptualization. **Haokang Zhang:** Writing – original draft, Validation, Investigation. **Jin Cao:** Formal analysis. **Yuyin Yan:** Writing – review & editing. **Bingyang Cao:** Writing – review & editing, Supervision, Project administration, Funding acquisition.

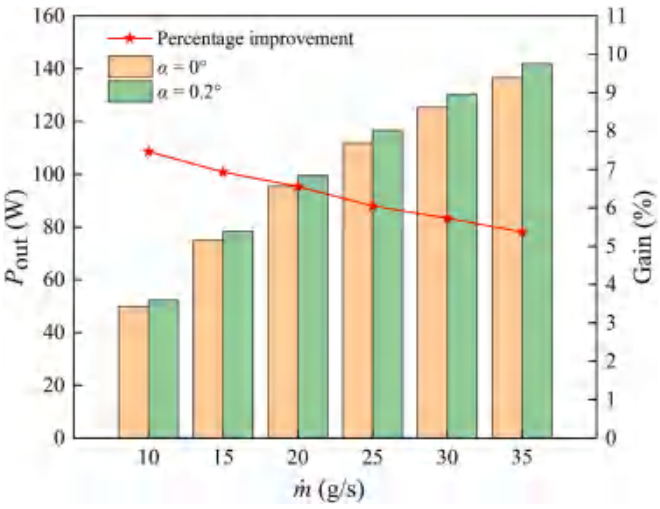

Fig. 13. Effect of mass flow rate on the performance gains under the optimal $\alpha = 0.2°$.

Declaration of competing interest

We declare that we do not have any commercial or associative interest that represents a conflict of interest in connection with the work submitted.

Data availability

Data will be made available on request.

Acknowledgements

This work was supported by the National Natural Science Foundation of China (Nos. 52250273, U20A20301), the National Natural Science Foundation of China (52306017), and the Natural Science Foundation of Hubei Province (No. 2023AFB093).

Appendix A. Supplementary data

Supplementary data to this article can be found online at https://doi.org/10.1016/j.energy.2024.131756.

References

[1] Yang W, Jin C, Zhu W, Xie C, Huang L, Li Y, et al. Innovative design for thermoelectric power generation: two-stage thermoelectric generator with variable twist ratio twisted tapes optimizing maximum output. Appl Energy 2024;363:123047.
[2] Zhao Y, Li W, Zhao X, Wang Y, Luo D, Li Y, et al. Energy and exergy analysis of a thermoelectric generator system for automotive exhaust waste heat recovery. Appl Therm Eng 2024;239:122180.
[3] O'Brien RC, Ambrosi RM, Bannister NP, Howe SD, Atkinson HV. Safe radioisotope thermoelectric generators and heat sources for space applications. J Nucl Mater 2008;377:506–21.
[4] Miao Z, Meng X, Liu L. Improving the ability of thermoelectric generators to absorb industrial waste heat through three-dimensional structure optimization. Appl Therm Eng 2023;228:120480.
[5] Cao J, Sun Y, Zhang D, Luo D, Zhang L, Chanajaree R, et al. Interfacial double-coordination effect guiding uniform electrodeposition for reversible zinc metal anode. Adv Energy Mater 2023:2302770. n/a.
[6] Cao J, Zhang D, Chanajaree R, Luo D, Yang X, Zhang X, et al. A low-cost separator enables a highly stable zinc anode by accelerating the de-solvation effect. Chem Eng J 2024;480:147980.
[7] Liu Y, Liang H, Yang L, Yang G, Yang H, Song S, et al. Unraveling thermal transport correlated with atomistic structures in amorphous gallium oxide via machine learning combined with experiments. Adv Mater 2023;35:2210873.
[8] Liu Z-K, Shen Y, Li H-L, Cao B-Y. Observation of ballistic-diffusive thermal transport in GaN transistors using thermoreflectance thermal imaging. Rare Met 2024;43:389–94.

[9] Yu Z-Q, Li M-T, Cao B-Y. A comprehensive review on microchannel heat sinks for electronics cooling. Int J Extrem Manuf 2024;6:022005.
[10] He W, Xu Q, Liu S, Wang T, Wang F, Wu X, et al. Analysis on data center power supply system based on multiple renewable power configurations and multi-objective optimization. Renew Energy 2024;222:119865.
[11] Liu Z, Cheng K, Wang Z, Wang Y, Ha C, Qin J. Performance analysis of the heat pipe-based thermoelectric generator (HP-TEG) energy system using in-situ resource for heat storage applied to the early-period lunar base. Appl Therm Eng 2023;218:119303.
[12] Miao Z, Meng X, Li X. Design a high-performance thermoelectric generator by analyzing industrial heat transfer. Appl Energy 2023;347:121403.
[13] Luo D, Yan Y, Li Y, Yang X, Chen H. Exhaust channel optimization of the automobile thermoelectric generator to produce the highest net power. Energy 2023;281:128319.
[14] Chen J, Wang R, Luo D, Zhou W. Performance optimization of a segmented converging thermoelectric generator for waste heat recovery. Appl Therm Eng 2022;202:117843.
[15] Hasan MN, Nayan N, Nafea M, Muthalif AGA, Mohamed Ali MS. Novel structural design of wearable thermoelectric generator with vertically oriented thermoelements. Energy 2022;259:125032.
[16] Iezzi B, Ankireddy K, Twiddy J, Losego MD, Jur JS. Printed, metallic thermoelectric generators integrated with pipe insulation for powering wireless sensors. Appl Energy 2017;208:758–65.
[17] Gayner C, Kar KK. Recent advances in thermoelectric materials. Prog Mater Sci 2016;83:330–82.
[18] Yang X, Wang C, Lu R, Shen Y, Zhao H, Li J, et al. Progress in measurement of thermoelectric properties of micro/nano thermoelectric materials: a critical review. Nano Energy 2022;101:107553.
[19] Zhao J, Xu W, Kuang Z, Long R, Liu Z, Liu W. Segmental material design in thermoelectric devices to boost heat-to-electricity performance. Energy Convers Manag 2021;247:114754.
[20] Shen Z-G, Liu X, Chen S, Wu S-Y, Xiao L, Chen Z-X. Theoretical analysis on a segmented annular thermoelectric generator. Energy 2018;157:297–313.
[21] Luo D, Wang R, Yu W, Zhou W. A novel optimization method for thermoelectric module used in waste heat recovery. Energy Convers Manag 2020;209:117320.
[22] Chen W-H, Liao C-Y, Hung C-I, Huang W-L. Experimental study on thermoelectric modules for power generation at various operating conditions. Energy 2012;45:874–81.
[23] Luo D, Wang R, Yu W, Sun Z, Meng X. Modelling and simulation study of a converging thermoelectric generator for engine waste heat recovery. Appl Therm Eng 2019;153:837–47.
[24] Yang W, Zhu W, Li Y, Zhang L, Zhao B, Xie C, et al. Annular thermoelectric generator performance optimization analysis based on concentric annular heat exchanger. Energy 2022;239:122127.
[25] Li B, Huang K, Yan Y, Li Y, Twaha S, Zhu J. Heat transfer enhancement of a modularised thermoelectric power generator for passenger vehicles. Appl Energy 2017;205:868–79.
[26] Zhao Y, Zhang G, Wen L, Wang S, Wang Y, Li Y, et al. Experimental study on thermoelectric characteristics of intermediate fluid thermoelectric generator. Appl Energy 2024;365:123263.
[27] Yang W, Zhu W, Du B, Wang H, Xu L, Xie C, et al. Power generation of annular thermoelectric generator with silicone polymer thermal conductive oil applied in automotive waste heat recovery. Energy 2023;282:128400.
[28] Zhu W, Xu A, Yang W, Xiong B, Xie C, Li Y, et al. Optimal design of annular thermoelectric generator with twisted tape for performance enhancement. Energy Convers Manag 2022;270:116258.
[29] Li Y, Wang S, Zhao Y, Yue L. Effect of thermoelectric modules with different characteristics on the performance of thermoelectric generators inserted in the central flow region with porous foam copper. Appl Energy 2022;327:120041.
[30] Chen W-H, Chiou Y-B, Chein R-Y, Uan J-Y, Wang X-D. Power generation of thermoelectric generator with plate fins for recovering low-temperature waste heat. Appl Energy 2022;306:108012.
[31] Yang W, Jin C, Zhu W, Li Y, Zhang R, Huang L, et al. Taguchi optimization and thermoelectrical analysis of a pin fin annular thermoelectric generator for automotive waste heat recovery. Renew Energy 2024;220:119628.
[32] Chen W-H, Wang C-M, Huat Saw L, Hoang AT, Bandala AA. Performance evaluation and improvement of thermoelectric generators (TEG): fin installation and compromise optimization. Energy Convers Manag 2021;250:114858.
[33] Zhang Z, Chen LN, Chen ZJ, Xiao GQ, Liu ZJ. Structure and output characteristics of a TEM array fitted to a fin heat exchanger. J Electron Mater 2015;44:2186–91.
[34] Meng J-H, Wang X-D, Chen W-H. Performance investigation and design optimization of a thermoelectric generator applied in automobile exhaust waste heat recovery. Energy Convers Manag 2016;120:71–80.
[35] Luo D, Liu Z, Yan Y, Li Y, Wang R, Zhang L, et al. Recent advances in modeling and simulation of thermoelectric power generation. Energy Convers Manag 2022;273:116389.
[36] Luo D, Yang S, Yan Y, Cao J, Cao B. Performance improvement of the automotive thermoelectric generator by extending the hot side area of the heat exchanger through heat pipes. Energy Convers Manage 2024;310:118472.
[37] Bai W, Yuan X, Liu X. Numerical investigation on the performances of automotive thermoelectric generator employing metal foam. Appl Therm Eng 2017;124:178–84.
[38] Luo D, Wang R, Yu W, Zhou W. Performance optimization of a converging thermoelectric generator system via multiphysics simulations. Energy 2020;204:117974.
[39] Luo D, Wang R, Yu W, Zhou W. A numerical study on the performance of a converging thermoelectric generator system used for waste heat recovery. Appl Energy 2020;270:115181.
[40] Fernández-Yañez P, Armas O, Capetillo A, Martínez-Martínez S. Thermal analysis of a thermoelectric generator for light-duty diesel engines. Appl Energy 2018;226:690–702.
[41] Kim TY, Kwak J, Kim B-w. Energy harvesting performance of hexagonal shaped thermoelectric generator for passenger vehicle applications: an experimental approach. Energy Convers Manag 2018;160:14–21.
[42] Chen W-H, Lin Y-K, Luo D, Jin L, Hoang AT, Saw LH, et al. Effects of material doping on the performance of thermoelectric generator with/without equal segments. Appl Energy 2023;350:121709.
[43] Xu A, Xie C, Xie L, Zhu W, Xiong B, Gooi HB. Performance prediction and optimization of annular thermoelectric generators based on a comprehensive surrogate model. Energy 2024;290:130195.
[44] Luo D, Wu Z, Yan Y, Cao J, Yang X, Zhao Y, et al. Performance investigation and design optimization of a battery thermal management system with thermoelectric coolers and phase change materials. J Clean Prod 2024;434:139834.
[45] Luo D, Yan Y, Li Y, Wang R, Cheng S, Yang X, et al. A hybrid transient CFD-thermoelectric numerical model for automobile thermoelectric generator systems. Appl Energy 2023;332:120502.
[46] Luo D, Zhao Y, Cao J, Chen W-H, Zhao Y, Cao B. Performance analysis of a novel thermoelectric-based battery thermal management system. Renew Energy 2024;224:120193.
[47] Luo D, Sun Z, Wang R. Performance investigation of a thermoelectric generator system applied in automobile exhaust waste heat recovery. Energy 2022;238:121816.
[48] Luo D, Yan Y, Chen W-H, Cao B. Exploring the dynamic characteristics of thermoelectric generator under fluctuations of exhaust heat. Int J Heat Mass Transfer 2024;222:125151.
[49] Lu X, Yu X, Qu Z, Wang Q, Ma T. Experimental investigation on thermoelectric generator with non-uniform hot-side heat exchanger for waste heat recovery. Energy Convers Manag 2017;150:403–14.